Quantum fidelity of the Aubry-André model and the exponential orthogonality catastrophe

J. Vahedi [1,*] and S. Kettemann [1,2,†]

[1]*Department of Physics and Earth Sciences, Jacobs University Bremen, Bremen 28759, Germany*

[2]*Division of Advanced Materials Science, Pohang University of Science and Technology (POSTECH), Pohang 790-784, South Korea*

(Received 3 August 2022; revised 12 November 2022; accepted 16 November 2022; published 30 November 2022)

Advances in experimental tools allow to study quantum fidelity in unprecedented controlled settings. While the fidelity in metals, when adding a local impurity, is well known to show the Anderson orthogonality catastrophe (AOC), there remain outstanding questions in other quantum phases and settings. Here, we aim to tackle these by exploring systematically the ground-state fidelity of the Fermi liquid in the (extended) Aubry-André (AA) model, which allows to explore the AOC in both localized extended and critical phases. We discover that the AOC is typically exponential in the critical regime of the AA model and at the mobility edge of the extended AA model for an extended impurity, while it decays in the AA model with a power law for a weak single-site impurity. We explain this in terms of critical correlations and multipoint correlations. The OC is found to be exponential in the insulating regime, due to a fundamentally different, statistical mechanism, which is explained in detail. Furthermore, we consider a parametric perturbation to the AA model, and find an exponential OC numerically, in agreement with an analytical derivation which we provide here.

DOI: 10.1103/PhysRevB.106.174204

I. INTRODUCTION

The quantum fidelity F, the absolute value of the scalar product between the ground state of a quantum system $|\psi\rangle$ and the ground state after a perturbation $|\psi'\rangle$, at fixed density of fermions $n = N/L^d$, $F = |\langle\psi|\psi'\rangle|$ is known to vanish with a power law of the system size L in a metallic phase, the celebrated Anderson orthogonality catastrophe [1]. Anderson showed in Ref. [1] that the fidelity has a strict upper bound

$$F = |\langle\psi \mid \psi'\rangle| < \exp(-I_A), \tag{1}$$

where the Anderson integral I_A is for noninteracting electrons given in terms of the single-particle eigenstates of the original system $|n\rangle$ and the new system $|n'\rangle$ by

$$I_A = \frac{1}{2}\sum_{n=1}^{N}\sum_{n'>N} |\langle n|n'\rangle|^2. \tag{2}$$

If the added impurity is short ranged of strength V_0, Anderson found for a clean metal $I_A = (1/2)\rho_0^2 V_0^2 \ln N$, diverging with the number of fermions N, where ρ_0 is the density of states at the Fermi energy. Therefore, F decays in metals as a power law of $N = nL^d$, the so-called Anderson orthogonality catastrophe (AOC). According to Eq. (2) this suppression is a consequence of the fact that the local perturbation connects the Fermi liquid to the continuum of excited states in the metal. This has important experimental consequences like the singularities in x-ray absorption and emission of metals [3], the zero-bias anomaly in disordered metals [4], and anomalies in the tunneling density of states in quantum Hall systems [5,6]. In particular, for compressible quantum Hall states, where there are edge channels propagating in both directions, there are AOC-type corrections to the tunneling density of states [6]. The concept of fidelity can be generalized to any parametric perturbation and be used to characterize quantum phase transitions [7], which have been applied to identify topologically different quantum phases in fractional quantum Hall phases [8]. A relationship between the orthogonality catastrophe and the adiabaticity breakdown in a driven many-body system has been shown in Ref. [9]. We note that, in general, the study of quantum quench dynamics requires to study the effect of the perturbation on all states [10], while we focus in this paper on the fidelity of the ground state. This AOC in the fidelity of the ground state can be studied in ensembles of ultracold atoms in a controlled way [11].

Recently, it has been found that the AOC with a local impurity can be exponential, meaning an exponential dependence of the typical fidelity on the number of fermions N at any quantum-critical point, as obtained in an analytical derivation [12]. There, the coupling to a continuum of excited states due to the impurity was found to be enhanced by quantum-critical power-law correlations. On the other hand, it has been argued in Refs. [13] and [12] that in an Anderson insulator the fidelity with a local impurity remains typically finite since the impurity can couple only to a discrete number of states. In Refs. [14,15], however, an exponential AOC was found numerically in Anderson-localized Fermi systems, when the perturbation is turned on adiabatically slowly.

In order to clarify the existence of an exponential AOC, here we aim to study the fidelity in the (extended) quasicrystalline Aubry-André (AA) model [2,16,17]. The AA model has a quantum phase transition from a metal to a localized phase as function of parameter λ and a quantum-critical point $\lambda = 2$ [see Fig. 1 (left) where all eigenstates are known to be multifractal [17]]. In contrast to the Anderson metal-insulator transition in disordered systems, the model has a fractal energy spectrum, where the level spacing Δ scales with system

*j.vahedi@jacobs-university.de
†s.kettemann@jacobs-university.de

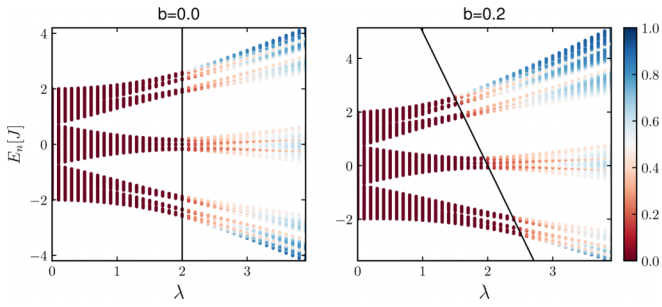

FIG. 1. The inverse participation ratio IPR $= \sum_i |\psi_i|^4$ as function of energy (in units of hopping parameter J) and quasiperiodicity parameter λ for the AA model (left) and EAA model with $b = 0.2$ (right). For the system size $L = 610$ a crossover is seen in the IPR between an extended phase IPR $\to 0$ (red) and a localized phase IPR $\to a/\xi$, with localization length ξ and lattice spacing a. In the AA model (left) that occurs at $\lambda = 2$ for all energies, while in the EAA model it depends on energy. There, the analytical result for the mobility edge $E_{\rm mb} = (2Jlambda)/b$ [2] (black solid line) is plotted, separating the extended phase from the localized phase.

size L with a fractal dimenison $z \neq 1$. In a recent study [18] the AOC at the critical point of this model has been studied and found numerically to follow a power law. This is another motivation for us to reconsider the fidelity in this model and to examine whether the exponential AOC predicted in Ref. [12] at a quantum-critical point exists in the critical AA model. Moreover, this model and its extensions can be realized in ultracold atoms, allowing the tuning of parameters and perturbations in a controlled way [11]. We summarize all results for the fidelity in Table I.

The paper is organized as follows. In Sec. II we introduce the (extended) AA model. In Sec. III we review the definition of ground-state fidelity F in the presence of an impurity and its upper bound provided by the exponential of the Anderson integral (AI). In Sec. IV we define the AI with an extended impurity. In Sec. V we review the spectrum of the AA model and study how it is modified by an impurity. In Sec. VI we present all results for the fidelity of a single-site impurity in the AA model. We begin with presenting the numerical results in Sec. VI A. The analytical results in the approximation used in Ref. [12] are reviewed and applied for the AA model with a single-site impurity in Sec. V B yielding an exponential AOC in the critical phase. As this is in some disagreement with the numerical results presented in Sec. VI A, we consider corrections to the AI in Sec. VI C beyond the approximation used in Sec. VI B. We thereby identify a mechanism which yields a power-law AOC in the critical phase, in agreement with the numerical results. In Sec. VI D we show that in the insulator regime there is a statistical mechanism which yields an exponential OC in agreement with the numerical results. In Sec. VII we present results for the fidelity with an extended impurity and provide evidence for an exponential AOC in the critical regime, when the impurity extends over more than one site. By analyzing the Anderson integral for an extended impurity we suggest a mechanism which explains this discovery of an exponential AOC in the critical phase. In Sec. VIII we present numerical results for the ground-state fidelity with a parametric perturbation giving evidence for an exponential AOC in the critical regime, and a weak exponential AOC in the metallic regime. Analyzing the Anderson integral for that perturbation we give a derivation which is in agreement with these numerical results. In Sec. IX we present numerical results for the ground-state fidelity in the extended AA model. We give the conclusions in Sec. X. In Appendix A we give the derivation of an upper bound for the ground-state fidelity and in Appendix B details of the derivation of the AOC with a single-site impurity. In Appendix C we present numerical benchmark results for the fidelity of the one-dimensional (1D) tight-binding model with an impurity. In Appendix D we present the averaged numerical results for the energy spectrum of the AA model with a single-site impurity.

II. THE (EXTENDED) AUBRY-ANDRé-MODEL

The (extended) Aubry-André model (EAA) has the Hamiltonian [2,16]

$$H_{\rm EAA} = -J \sum_{i=1}^{L} (c_i^+ c_{i+1} + c_{i+1}^+ c_i) + \lambda \sum_{i=1}^{L} \frac{\cos(2\pi Q i + \phi)}{1 - b\cos(2\pi Q i + \phi)} c_i^+ c_i, \qquad (3)$$

TABLE I. Summary of results for the length L dependence of fidelity F in loc = localized, ext = extended, crit= critical phase of the AA = Aubry-André model and the EAA = extended AA model with imp=impurity. c is a constant, exponent γ is numerically found to be $\gamma \approx 1$, analytically $\gamma = z/2$, with $z > 1$ the fractal dynamical exponent. The exponent β is determined by fitting, as given in the respective figures. In addition, the average fidelity is found to be independent of L in the localized regime for single-site and extended impurities [see Fig. 8(c)] and for a parametric perturbation (see Fig. 13).

Fidelity $F(L)$	Exponential $\sim \exp(-cL^\gamma)$	Power law $\sim L^{-\beta}$
AA + single-site imp $M = 1$	loc: $F_{\rm typ}$ (Fig. 5) crit: $F_{\rm typ}$ [Fig. 11(b)], $F_{\rm av}$ [Fig. 12(b)]	crit: $F_{\rm typ}$ (Fig. 5), $F_{\rm av}$ (Fig. 3) ext: $F_{\rm typ}$ (Fig. 5), $F_{\rm av}$ [Fig. 8(a)]
AA + ext imp $M > 1$	loc: $F_{\rm typ}$ [Fig. 11(c)]	ext: $F_{\rm typ}$ [Figs. 7(a),11(a)], $F_{\rm av}$ [Figs. 8(a),12(a)]
AA + parametric perturbation	crit, ext: $F_{\rm typ}$, $F_{\rm av}$ (Fig. 13)	
EAA + single-site imp	crit: $F_{\rm typ}$ [Fig. 14(a)], loc: $F_{\rm typ}$	crit: $F_{\rm av}$ [Fig. 14(a)], ext
EAA + ext imp	crit: $F_{\rm typ}$ (Fig. 15), loc: $F_{\rm typ}$	ext
1D tight-binding model + single-site imp		ext: $F_{\rm typ}$ $F_{\rm av}$ (Fig. 17)
1D tight-binding model + ext imp		ext: $F_{\rm typ}$, $F_{\rm av}$ (Figs. 18, 19)

where J is the hopping amplitude (we set $J = 1$ as the unit of energy), $c_i^\dagger$ and c_i are creation and annihilation operators of a spinless fermion at site i on a chain of L sites, and λ presents the amplitude of the quasiperiodic potential. Q is an irrational number usually chosen to be the golden ratio, $Q = 2/(\sqrt{5}+1)$, and ϕ is a randomly chosen phase interval $[0, 2\pi]$ that is the same for all sites. The open boundary conditions are considered throughout the results presented in the paper. The parameter b can take values $b \in [0, 1)$. For $b = 0$ we recover the Aubry-André model, which has no mobility edge in the energy spectrum, but when the parameter λ is changed all states undergo a transition from localized $\lambda > 2$, critical $\lambda = 2$, to extended for $\lambda < 2$ [16], as seen in Fig. 1 (left), where the inverse participation ratio (IPR $= \sum_i |\psi_i|^4$) is plotted versus energy and parameter λ. At the critical point $\lambda_c = 2$, all eigenstates are known to be multifractal [17]. Moreover, the model has a fractal energy spectrum, where the level spacing Δ scales with system size L as z, $\Delta \sim L^{-z}$, where the dynamical exponent z can be different from the dimension of the model $d = 1$.

For $b \neq 0$ the EAA model shows a mobility edge given by $E_{\rm mb} = (2J - \lambda)/b$ [2], as seen in Fig. 1 (right), where the inverse participation ratio (IPR) is plotted as function of energy and parameter λ. The mobility edge (black solid line) separates the extended phase IPR $\to 0$ from the localized IPR $\to a/\xi$, where a is the lattice spacing and ξ the localization length.

III. GROUND-STATE FIDELITY

To derive the ground-state fidelity we first diagonalize the Hamiltonian as given by Eq. (3). As the model is noninteracting, it can be diagonalized with the basis change as $H_{\rm AA} = \sum_n \epsilon_n d_n^\dagger d_n$, with the one-electron energy eigenvalues ϵ_n, and the creation and annihilation operators in the single-particle eigenstates $|n\rangle$ given by $d_n = \sum_i \psi_{ni} c_i$, where ψ_{ni} are complex coefficients. Then, the ground state can be constructed as $|\psi\rangle = \prod_{n=1}^N d_n^\dagger |0\rangle$, with fixed number of particles N and fixed particle filling $n = N/L$. When adding a perturbation the filling n remains fixed, while the Fermi energy can change.

Next, we introduce an impurity, which extends over a finite subset S_M of M neighbored lattice sites with $S_M = i, i+1, \ldots, i+M-1$ with

$$H_{\rm imp} = \frac{1}{M} V_0 \sum_{i \in S_M} c_i^+ c_i. \tag{4}$$

In the numerical implementation we choose the center of the impurity to be located at the lattice center $L/2$. The noninteracting Hamiltonian perturbed by the impurity $H' = H_{\rm AA} + H_{\rm imp}$ has the new eigenstates $|n'\rangle$, yielding $H' = \sum_{n'} \epsilon'_{n'} d_{n'}^\dagger d_{n'}$, where $d_{n'} = \sum_i \psi_{n'i} c_i$, with complex coefficients $\psi_{n'i}$. Thereby, the new ground state is given by $|\psi'\rangle = \prod_{n'=1}^N d_{n'}^\dagger |0\rangle$. Thus, the fidelity is given by $F = |\langle\psi'|\psi\rangle| = |\det(A)|$, where A is the $N \times N$ matrix where the matrix elements are the scalar products of the eigenstates before and after the perturbation $A_{nn'} = \langle n|n'\rangle$ (see Appendix A for more details).

IV. ANDERSON INTEGRAL

Before presenting the numerical results, let us first review the rigorous upper limit of the fidelity, as given by the right-hand side of Eq. (1), whose derivation is given in Appendix A. The Anderson integral (2) can be rewritten for the impurity perturbation (4) without approximation as

$$\begin{aligned} I_A &= \frac{1}{2} \sum_{n=1}^N \sum_{n'>N} \frac{1}{(E_{n'} - E_n)^2} |\langle n|H_{\rm imp}|n'\rangle|^2 \\ &= \frac{V_0^2}{2M^2} \sum_{n=1}^N \sum_{n'>N} \frac{|\sum_{i \in S_M} \psi_{ni}^* \psi_{n'i}|^2}{(E_{n'} - E_n)^2}, \end{aligned} \tag{5}$$

where $\psi_{ni} = \langle n|i\rangle$, $\psi_{n'i} = \langle n'|i\rangle$ is the local amplitude with and without the additional impurity at site i. Equation (5) can be rewritten by replacing the summation over energy eigenvalues $E_{n'}$, E_n by an integral over energy with density of states $\rho(E)$ without the impurity, and $\rho'(E')$ with the impurity. Thus, we get

$$\begin{aligned} I_A = \frac{V_0^2}{2M^2} \int_{E \leqslant \epsilon_{\rm HOMO}} dE \int_{E' \geqslant \epsilon'_{\rm LUMO}} dE' \frac{\rho(E)\rho'(E')}{(E_{n'} - E_n)^2} \\ \times \sum_{i,j \in S_M} \psi_{Ei}^* \psi_{E'i} \psi_{Ej} \psi_{E'j}^*, \end{aligned} \tag{6}$$

which depends explicitly both on the density of states (DOS) with and without impurity, $\rho'(E')$, $\rho(E)$, and on the wave-function amplitudes with and without the impurity $\psi_{E'i}$, ψ_{Ei}. We note that, since the number of fermions N is kept fixed, the Fermi energy of the pure system ϵ_F can be different from the one of the system with the perturbation ϵ'_F since all energy levels $E_{n'}$ may change with the perturbation. We therefore find it convenient to define the highest occupied energy level without the perturbation as $\epsilon_{\rm HOMO}$ and the lowest unoccupied energy level with the perturbation as $\epsilon'_{\rm LUMO}$. We note that Eq. (6) is still an exact representation of the Anderson integral, rewritten in terms of the density of states. As the density of states of the AA model is known to show fractal behavior at the critical point $\lambda_c = 2$, let us first consider the effect of the impurity on the energy spectrum.

V. ENERGY SPECTRUM

In Fig. 2(a) we show the energy level spectrum of the AA model [Eq. (3)] for $b = 0$ and the critical parameter $\lambda_c = 2.0$ as function of filling factor n. The dashed line indicates the filling of $n = 0.309$, corresponding without an impurity to the Fermi energy $E_F/J = -1.923$. In the inset the zoomed energy interval close to that filling $n = 0.309$ is seen to correspond to a region of large density of states. For a single-site impurity the energy level spectrum is plotted for three different impurity strengths V_0 as displayed by the colored symbols, respectively. Figures 2(b) and 2(c) show a full and zoomed energy level diagram, with and without impurity. The case without impurity is drawn in a gray color. While the energy bands are not shifted, the formation of bound states outside of the energy bands is seen even for the weakest impurity strength. Figure 2(d) shows the density of state (DOS) as a function of energy close to Fermi energy. The results

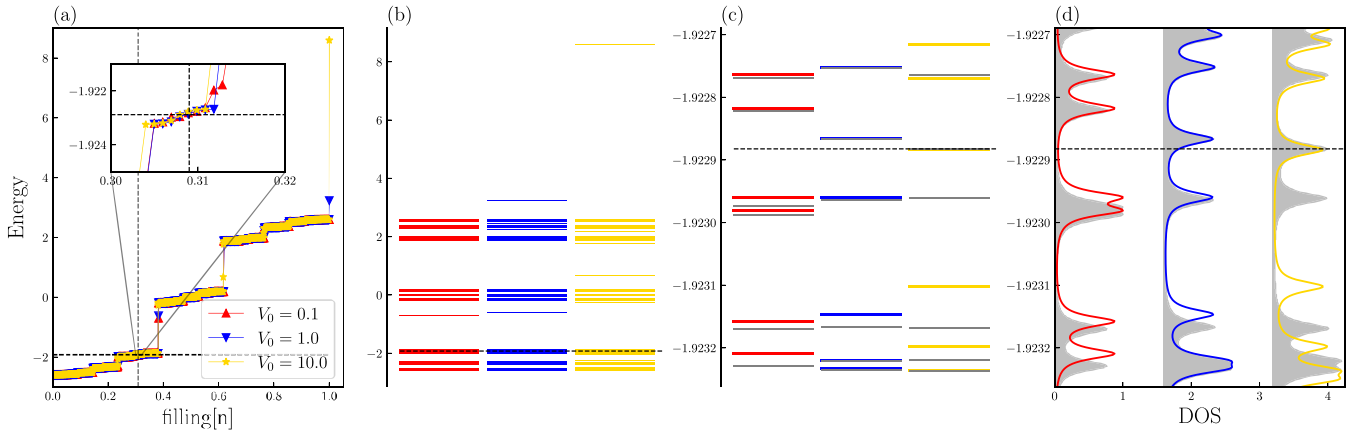

FIG. 2. (a) Energy spectrum at the critical point $\lambda = 2.0$ as function of filling n for a single-impurity case. Results of three different impurity strengths V_0 are displayed in colored symbols. The energy bands are not shifted, but bound states form outside of the energy bands for all V_0. The horizontal dashed line is the Fermi energy. Inset: zoomed energies close to the Fermi energy without the impurity $E_F/J = -1.922\,882$, corresponding to filling $n = 0.309$. (b), (c) Show the complete energy diagram, and a zoom close to the E_F, with and without (gray) impurity. (d) Density of states (DOS) as function of energy close to E_F. The results are randomly chosen from one of the realizations. For calculating DOS a broadening $\eta = 1.0 \times e^{-5}$ is utilized. System size $L = 1024$.

presented here are randomly chosen from one of the realizations. For the calculation of the DOS, a broadening $\eta = 1. \times e^5$ has been used.

Figure 20 in Appendix D shows the average density of states as function of energy E, as averaged over the random phases ϕ in the Hamiltonian (3) for $b = 0$ and $\lambda = 2$ of 200 realizations. This supports the observation that the energy bands are not shifted by more than a level spacing, and that the formation of bound states outside of the energy bands is seen even for the weakest impurity strength.

VI. GROUND-STATE FIDELITY OF THE AA MODEL WITH A SINGLE-SITE IMPURITY

A. Numerical results

Let us first consider the fidelity in the 1D Aubry-André model with Hamiltonian (3) for $b = 0$, for a single-site impurity $M = 1$ [Eq. (4)] numerically. Calculating the fidelity, using its definition $F = |\langle\psi'|\psi\rangle|$, we plot in Figs. 3(a) and 3(b) the average fidelity $F_{\text{ave}} = \langle F\rangle$ and the typical fidelity as function of length L for different impurity strengths $V_0 = 0.1, 0.01$. Here, we defined $F_{\text{typ}} = \exp\langle\log F\rangle$, where $\langle\dots\rangle$ denotes the average over 1000 realizations of a uniform random phase in $[0, 2\pi)$. We find that both the average and the typical fidelity decay with a power law, and not exponentially. The typical fidelity is smaller than the average one for all system sizes L. This difference becomes more pronounced with stronger impurity strength V_0, while the fidelity becomes smaller with increasing V_0 overall. For comparison, we also calculated the Anderson integral I_A, and plot in Figs. 3(c) and 3(d) the average of its exponential $\langle\exp(-I_A)\rangle$, which should give according to Eq. (1) the upper bound of the average fidelity, and the exponential of the average I_A, $\exp(-\langle I_A\rangle)$, which corresponds to the upper bound for the typical fidelity. Indeed, we confirm the inequality (1) for both impurity strengths $V_0 = 0.1, 0.01$. But, we observe that the typical fidelity F_{typ} is substantially smaller than its upper bound $\exp(-\langle I_A\rangle)$.

B. Anderson integral: Analytical results

These numerical results are in contradiction with the prediction of an exponential orthogonality catastrophe, as found by an analytical derivation in Ref. [12] at a quantum-critical point, where the coupling to a continuum of excited states due to the impurity was found to be enhanced by quantum-critical power-law correlations. Let us therefore reconsider the derivation of the Anderson integral for critical states.

In fact, in the critical regime all wave functions are multifractal [19] and the correlation function of intensities

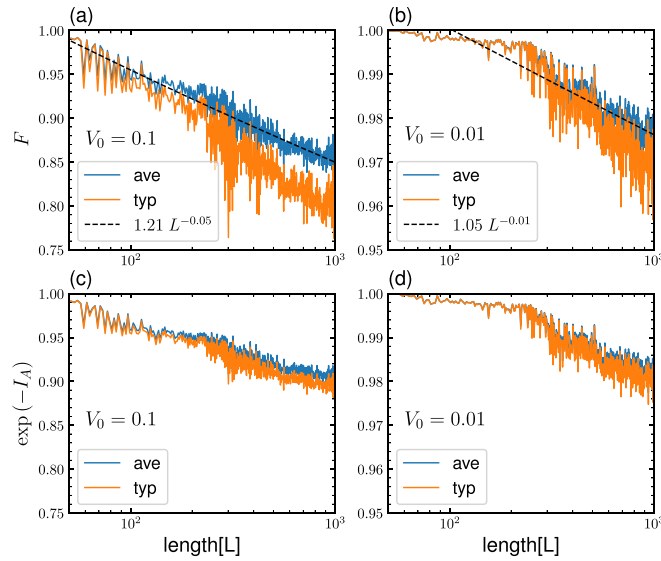

FIG. 3. (a) Average and typical fidelities as function of length L with a single impurity of strength $V_0 = 0.1$ and (b) for $V_0 = 0.01$, showing a power-law dependence on L, which is fitted as given in the legend. (c) Average and typical values of $\exp(-I_A)$, which is confirmed to exceed the typical fidelity, where I_A is the Anderson integral (5) for $V_0 = 0.1$ and (d) for $V_0 = 0.01$. Parameter $\lambda_c = 2.0$, data averaged over 1000 sample realizations.

associated to two energy levels distant in energy by $\omega_{nm} = E_n - E_m$ is enhanced, as given by [20–22]

$$C(\omega_{nm} = E_n - E_m) = L^d \int d^d r \, \langle |\psi_n(\mathbf{r})|^2 |\psi_m(\mathbf{r})|^2 \rangle = \begin{cases} \left(\frac{E_c}{\mathrm{Max}(|\omega_{nm}|, \Delta)}\right)^{\eta/d}, & 0 < |\omega_{nm}| < E_c \\ (E_c/|\omega_{nm}|)^2, & |\omega_{nm}| > E_c \end{cases} \quad (7)$$

where Δ is the average level spacing at the Fermi energy. The power is given by $\eta = 2(\alpha_0 - d)$, with multifractality parameter α_0 and the dimension d. This power-law dependence of the correlation function is a consequence of multifractality, as can be seen in the limit when $|E_n - E_m| < \Delta$ where it becomes L^d times the inverse participation ratio which is known to scale as L^{-d_2}, where d_2 is the fractal dimension of the second moment of the intensity, given by $d_2 = d - \eta$. For the critical AA model, the power is known to be $\eta = \frac{1}{2}$ [23]. Since all its states are critical, the correlation energy E_c is of order of the bandwidth D. For $|\omega_{nm}| < E_c$ correlations are thus indeed enhanced in comparison to the plane-wave limit $C_{nm} = 1$. Note that for $|\omega_{nm}| > E_c$ it decays below 1.

Mean value of the Anderson integral. If we assume that the perturbed eigenstates $\langle n'|$ in Eq. (5) can be replaced by an eigenstate without the impurity $\langle n|$, we can insert the correlation function (7) into (5) to calculate the mean value of I_A, and find for a single-site impurity $M = 1$

$$\langle I_A \rangle = \frac{V_0^2}{2} \iint_{\epsilon < \epsilon_{\mathrm{Homo}}, \epsilon' > \epsilon_{\mathrm{Lumo}}} d\epsilon \, d\epsilon' \rho(\epsilon) \rho(\epsilon') \frac{C_{\epsilon,\epsilon'}}{(\epsilon - \epsilon')^2}. \quad (8)$$

This gives an estimate for the upper bound of the typical average of F, $\exp(\langle \ln F \rangle) \leqslant \exp(-\langle I_A \rangle)$. Assuming furthermore that the density of states is only slowly varying $\rho(E) \approx \rho(E_F) = \rho_0$, and denoting the level spacing at the Fermi energy $\Delta = \epsilon_{\mathrm{Lumo}} - \epsilon_{\mathrm{Homo}}$, we get at the Anderson metal-insulator transition (AMIT) with Eq. (7)

$$\langle I_A \rangle|_{E_F = E_M} = \frac{(\rho_0 V_0)^2}{2\gamma(1+\gamma)} \left(\frac{E_c}{\Delta}\right)^{\gamma}, \quad (9)$$

depending on E_c/Δ with power $\gamma = \eta/d$. For the critical phase of the one-dimensional AA model, $d = 1$, $\gamma = \frac{1}{2}$ [23].

Since all states are critical at $\lambda = 2$, we set the correlation energy to the bandwidth $E_c = D$. In a metal the average level spacing is $\Delta = 1(\rho_0 L)$. Note, however, that for the fractal spectrum of the AA model, the level spacing at the Fermi energy scales with L rather as $\Delta(L) \sim L^{-z}$, with $z > 1$ [18]. Thereby, we get

$$\langle I_A \rangle|_{E_F = 0} = \frac{\rho_0^2 V_0^2}{2\gamma(1+\gamma)} (D \rho_0 L^z)^{\gamma}. \quad (10)$$

Thus, we get with $\gamma = \eta/d = \frac{1}{2}$, $\rho_0 = 1/D$, that the Anderson integral diverges as a power law with system size L,

$$\langle I_A \rangle|_{E_F = 0} = \frac{2V_0^2}{3D^2} L^{z/2}, \quad (11)$$

and thus the typical fidelity decays exponentially with the system size, the exponential orthogonality catastrophe, in agreement with Ref. [12].

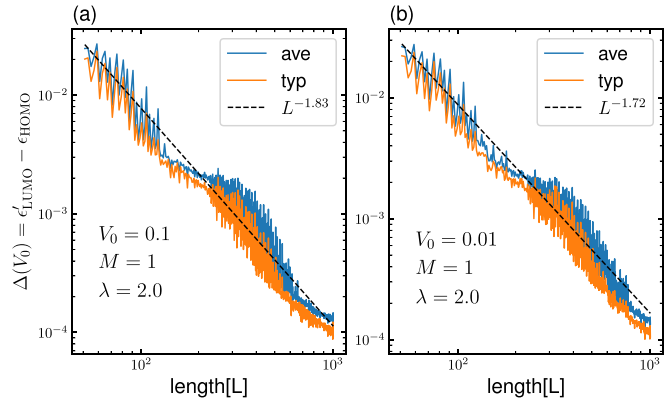

FIG. 4. Average and typical gap, the difference between HOMO and LUMO energies [Eq. (13)] of the model before and after the perturbations were considered for two different single-impurity strengths (a) $V_0 = 0.1$ and (b) $V_0 = 0.01$ as function of length L. This confirms the power-law dependence with a power $z > 1$ exceeding the dimension $d = 1$, which is due to the fractality of the spectrum. In all results, we fix parameter $\lambda = 2.0$ and data averaged over 1000 sample realizations.

In the metallic regime $\lambda < 2$ one rather gets

$$\langle I_A^M \rangle|_{E_F = 0} = \frac{\rho_0^2 V_0^2}{2} \ln(D \rho_0 L). \quad (12)$$

Thus, in order to be able to distinguish the exponential decay of the typical fidelity due to critical correlations, Eq. (11) in comparison to the noncritical result (12), the system size L should be so large that $4/3L^{z/2} > \ln L$ which is indeed valid for all $L > 1$ for $z > 1$. Thus, according to this result, the numerical calculations should see the exponential decay, if the analytical derivation is valid. Therefore, let us reconsider the approximations yielding to the result (10), in order to find out the reason for this discrepancy with the numerical results.

C. Anderson integral: Beyond perturbation theory

(1) As the energy levels are modified by the perturbation, the gap between the lowest unoccupied state with the perturbation and the highest occupied level without perturbation depends itself on the disorder potential V_0,

$$\Delta(V_0) = \epsilon'_{\mathrm{LUMO}} - \epsilon_{\mathrm{HOMO}}. \quad (13)$$

Since it provides the infrared cutoff to the integrals in the Anderson integral, substituting Eq. (13) into (14) we thereby find in the critical phase

$$\langle I_A \rangle|_{E_F = E_M} = \frac{(\rho_0 V_0)^2}{2\gamma(1+\gamma)} \left(\frac{E_c}{\Delta(V_0)}\right)^{\gamma}. \quad (14)$$

In Fig. 4 the average and typical gap $\Delta(V_0)$ [Eq. (13)] is shown for two different single-impurity strengths, namely, (a) $V_0 = 0.1$ and (b) $V_0 = 0.01$ for critical parameter $\lambda = 2.0$ and data averaged over 1000 sample realizations. We see that the magnitude of the gap is not changed by the impurity, so that this weak dependence of $\Delta(V_0)$ on V_0 does not change the result for the Anderson integral (11).

Also, as was observed for the gap of the unperturbed system in Ref. [18], the decay with system size L of the gap

$\Delta(V_0)$ is strongly fluctuating with L and does not follow a clear scaling law, even when averaging over 1000 realizations. However, it clearly decays with a power $z > 1$, faster than the average level spacing of a metal.

(2) The density of states is affected by the presence of the impurity, as seen in Fig. 2 for a particular realization of the phase ϕ. As discussed in Sec. V, the energy bands are hardly shifted, but the formation of bound states outside of the energy bands is found even for the weakest impurity strength. Close to the Fermi energy Fig. 2(d) shows that the density of state (DOS) is only weakly shifted by the impurity, by the order of the level spacing Δ. As we choose an energy region of large density of states, which is not shifted on average by the impurity, as seen in Fig. 20, we conclude that the small change of DOS $\rho'(E)$ by the impurity does not result in a change of the divergence with system size L of the average Anderson integral in the critical regime, and thus cannot be responsible for the discrepancy with the numerical results.

(3) We disregarded in the derivation in Sec. VI B the change of wave-function intensity at the location of the impurity by the addition of the impurity. For a single-site potential impurity at site $\mathbf{x}$ with amplitude V_0, the perturbed intensity $|\psi_{n'}(\mathbf{x})|^2$ can be written exactly as [24]

$$|\psi_{n'}(\mathbf{x})|^2 = \lim_{E\to E_{n'}} (E - E_{n'}) \frac{V_0 \left[G_E^0(\mathbf{x},\mathbf{x})\right]^2}{1 - V_0 G_E^0(\mathbf{x},\mathbf{x})}, \tag{15}$$

where

$$G_E^0(\mathbf{x},\mathbf{x}) = \sum_l |\psi_l(\mathbf{x})|^2 \frac{1}{E - E_l + i\delta}. \tag{16}$$

Performing the limit in Eq. (15) with de l'Hospital rule, one finds

$$|\psi_{n'}(\mathbf{x})|^2 = |\psi_n(\mathbf{x})|^2 \frac{\left(1 + \frac{E_{n'}-E_n}{|\psi_n(\mathbf{x})|^2} \sum_{l\neq n} \frac{|\psi_l(\mathbf{x})|^2}{E_{n'}-E_l}\right)^2}{1 + \frac{(E_{n'}-E_n)^2}{|\psi_n(\mathbf{x})|^2} \sum_{m\neq n} \frac{|\psi_m(\mathbf{x})|^2}{(E_{n'}-E_m)^2}}, \tag{17}$$

where E_n is the energy level closest in energy to the perturbed energy $E_{n'}$. It depends on the disorder potential only implicitly through the eigenenergy of the perturbed state $E_{n'}$. Since $E_{n'} - E_n$ has a polynomial dependence on the disorder potential V_0, we can approximate it by the leading term, linear in V_0, $E_{n'} - E_n \approx V_0 |\psi_n(\mathbf{x})|^2$, yielding

$$|\psi_{n'}(\mathbf{x})|^2 \approx |\psi_n(\mathbf{x})|^2 \frac{\left(1 + V_0 \sum_{l\neq n} \frac{|\psi_l(\mathbf{x})|^2}{E_{n'}-E_l}\right)^2}{1 + V_0^2 |\psi_n(\mathbf{x})|^2 \sum_{m\neq n} \frac{|\psi_m(\mathbf{x})|^2}{(E_{n'}-E_m)^2}}. \tag{18}$$

Inserting this approximation into the Anderson integral, we can check whether these corrections in V_0 change the divergence of the Anderson integral. In the metal phase, $|\psi_n(\mathbf{x})|^2 \sim 1/L$ and due to the asymmetry of the summations in the numerator of Eq. (18), we find only weak corrections, which do not change the $\ln L$ dependence of the Anderson integral in the metallic regime. In the critical regime, however, all wave functions are multifractal, so that the local intensity $|\psi_l(\mathbf{x})|^2$ is widely distributed and may vary strongly with energy E_l. Then, the corrections due to the summations in Eq. (18) both in the numerator and denominator may yield finite results, especially when the intensity of the state at the Fermi energy at the location of the impurity $|\psi_n(\mathbf{x})|^2$ happens to be smaller than in other states. Inserting Eq. (18) into the Anderson integral, we see that multipoint correlations of the intensity arise even for the average Anderson integral. Thus, the average Anderson integral can in general not be reduced to an integral over the pair correlation function (7). The presence of multipoint correlation may therefore weaken the infrared divergence compared to Eq. (11). The numerical results shown in Fig. 3 in fact provide strong evidence that the Anderson integral depends on system size only logarithmically, resulting in a fidelity at the critical point which decays with a power law with system size, albeit decaying faster than in the metallic regime. Numerical results for the fidelity in the presence of an impurity in other quantum-critical systems, in particular in random banded matrices [25] and at the three-dimensional (3D) Anderson metal-insulator transition [26], did not find evidence for an exponential AOC either, but rather found evidence for a power-law AOC. As outlined above, the explanation may be that the corrections to the local intensity at a single-site impurity (18) result in multipoint correlations, which weaken the infrared singularity of the Anderson integral in these quantum-critical systems, thereby explaining the numerically observed power-law Anderson orthogonality catastrophe.

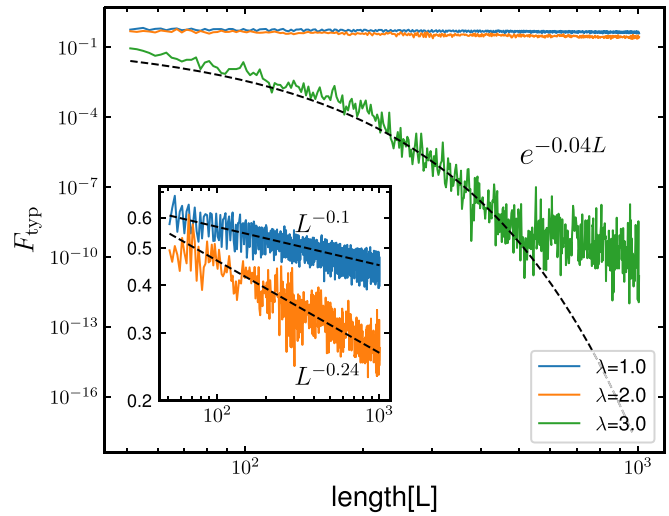

FIG. 5. Typical fidelity $F_{\rm typ} \approx \exp\langle \log F\rangle$ of a single impurity with strength $V_0/J = 20$ for $\lambda = 1$ (the metallic phase), $\lambda = 2$ (the critical phase), $\lambda = 3$ (the insulator phase) in log-log scale. This shows the power-law OC in the metallic and the critical phase and an exponential OC in the insulator phase. Filling is fixed at $n = 0.309$. The inset magnifies results of the main panel for $\lambda = 1.0, 2.0$. Results are averaged over 1000 samples. Black dashed lines are fitted curves.

D. Fidelity in the insulator phase: Statistical exponential orthogonality catastrophe

In Fig. 5 the typical fidelity $F_{\rm typ} = \exp\langle \log F\rangle$ of a strong single impurity with strength $V_0/J = 20$ is shown for the metallic $\lambda = 1.0$, the critical $\lambda_c = 2.0$, and the insulator $\lambda = 3.0$ regime. The filling is kept fixed at $n = 0.309$. All results are obtained by averaging over 1000 samples. We see that both in the metallic and the critical regime, the typical fidelity

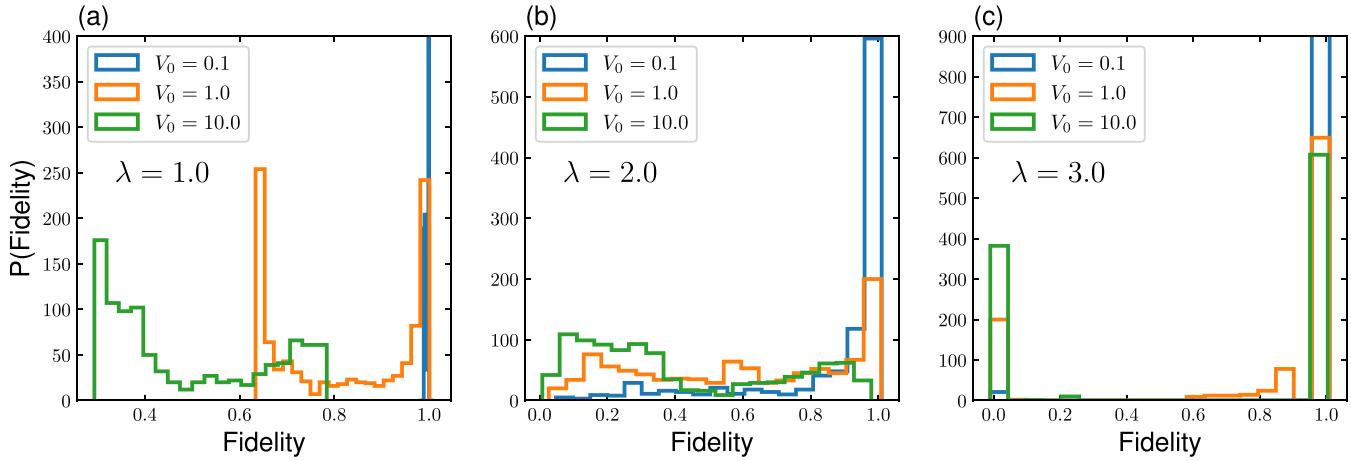

FIG. 6. Distribution of the fidelity for a single impurity $M = 1$ with different strengths V_0 for (a) metallic phase, where it has a finite width, is bimodal, and becomes shifted to smaller values as V_0 is increased. (b) Critical phase, where it spreads over all values of F, with more weight at small fidelity the larger V_0 is. (c) Localized phase, where it is bimodal. The peak at vanishing fidelity is increasing with impurity strength V_0, approaching a Bernoulli distribution, with only small weight at intermediate values. System size is $L = 1009$ and data are collected from 2000 realizations.

decays with system size like a power law, albeit the decay is faster in the critical regime. This is seen better in the inset where the dashed lines are fitted curves as indicated.

In the insulator regime $\lambda = 3.0$, however, the fidelity is by orders of magnitude smaller than that in the metallic and critical regimes. Moreover, it decays with system size L exponentially, as seen by the fitted dashed line, until it decays more slowly at system sizes exceeding $L = 500$. In Refs. [14,15], an exponential orthogonality catastrophe was found numerically in Anderson-localized Fermi systems, when the perturbation is turned on adiabatically slowly. In Ref. [14] that has been explained in terms of a *statistical* orthogonality catastrophe.

Indeed, in the strongly localized regime, when each eigenfunction is localized on one site only, one obtains a Bernoulli distribution of the fidelity of fixed particle number N, which is either 0 or 1 with probability u, $1 - u$, respectively. The reason is, that in this strongly localized regime a local impurity cannot mix eigenstates, but only shift the energy of that state, which is located at the site of the impurity. Thereby, for fixed number of particles the impurity may shift an occupied level to higher energies, leaving it unoccupied, while a state at another site becomes occupied, which is orthogonal to the state at the site of the impurity, or vice versa. Thus, by definition of the fidelity at fixed N, the fidelity is then exactly zero. If, on the other hand, the impurity shifts the energy such that the level remains occupied when it was occupied before, or leaving it unoccupied, when it was unoccupied without the impurity, the fidelity remains exactly one. Thus, one has a statistical distribution which has only two possible values, $S = 0$ with probability u or $S = 1$ with probability $1 - u$, where $u(V_0)$ is the probability that the impurity shifts the energy level at the site of the impurity from occupied to unoccupied states or vice versa. Thus, while the average fidelity is finite $\langle F \rangle = 1 - u$, the typical fidelity is vanishing, $\exp\langle \ln F \rangle = \exp[-\infty u + 0(1 - u)] = 0$. This statistical mechanism for the reduction of the typical fidelity is thereby completely different from the mechanism for the Anderson orthogonality catastrophe, where it is the coupling to a continuum of states in a metal which leads to the power-law suppression of the fidelity.

In Fig. 6 the distribution of the fidelity is shown in the metallic, the critical, and the insulator phase for three different impurity strengths. Indeed, in the insulator phase the distribution is bimodal, and the peak around zero fidelity is increasing with impurity strength V_0, approaching a Bernoulli distribution, with only small weight at intermediate values of the fidelity. In contrast, in the critical phase the distribution of F is very wide, spreading over all values of F, where the weight of small fidelity increases with V_0. The distribution of F in the metal phase on the other hand has a finite width, is bimodal, and becomes shifted to smaller F as V_0 is increased.

Having understood the distribution of F, let us next try to explain the exponential suppression of the fidelity with system size L in the insulator phase. As the filling factor $n = N/L$ is fixed as the system size L is increased, the number of occupied levels N increases. However, in the strongly localized regime, the probability that the single state at the site of the impurity is shifted from occupied to unoccupied levels or, vice versa, the probability u does not change with L since it is only a function of the impurity strength V_0, whether the energy level shift is sufficiently strong and the typical fidelity remains zero for all sizes. Thus, in the limit of strong single-site localization, the typical fidelity would be zero for all system sizes $L \gg 1$.

When the localization is not as strong, however, each localized state is extended over several sites, within the range of a localization length ξ. Thus, an impurity located within this range may mix the localized state with a finite number of other states. According to the Anderson mechanism, that would yield a finite fidelity on average, since an impurity can only be coupled to a finite number of states, which does not change as the system size increases. This is the reason that in Ref. [12] a finite typical fidelity, independent of the system size, has been found analytically. However, due to the statistical mechanism, which was not considered in Ref. [12], the impurity may shift an occupied state up in energy so that it becomes unoccupied, or vice versa. Then, another single-particle state becomes

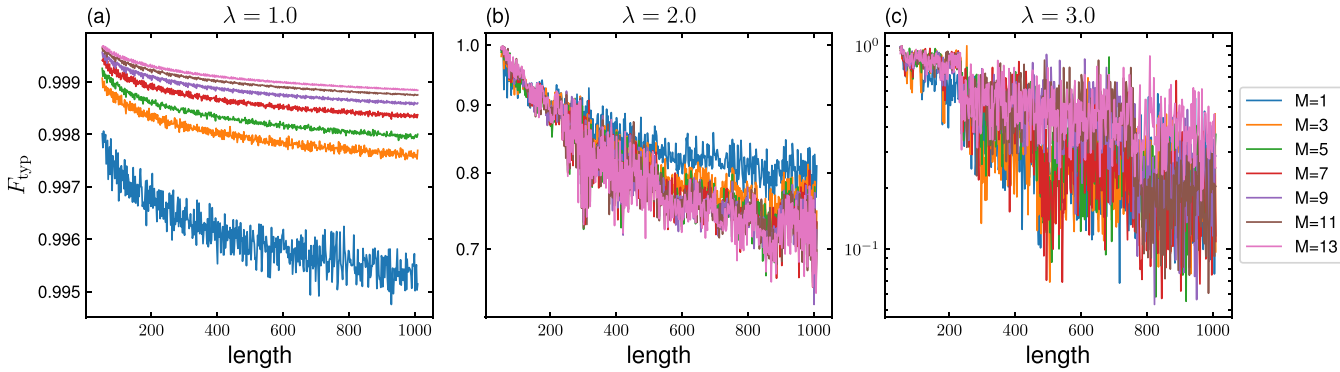

FIG. 7. Results for the typical fidelity at filling $n = 0.309$ as function of length L for different extensions of the impurity M are shown in color at fixed strength of the impurity $V_0 = 0.1J$, sampled over 1000 realizations for (a) the metallic phase $\lambda = 1$, where the fidelity is found to increase with extension M and to decay as a power law with length L, (b) the critical phase $\lambda = 2$, where the fidelity is found to rather decrease with extension M and to decay faster with length L the larger M, and (c) for the insulator phase $\lambda = 3$, where the fidelity is found to fluctuate strongly, being smallest for $M = 1$, and largest for the largest $M = 13$ considered and to decay faster with length L the smaller M.

occupied which may be (almost) orthogonal to the previously occupied state without the impurity. As the system size increases beyond a typical localization length ξ, the fidelity is decaying exponentially due to this statistical mechanism. As there are typically exponentially small but finite hybridization matrix elements between all sites, in reality the impurity may couple to a larger amount of states even though with exponentially small amplitude. This might explain that the typical fidelity seems to saturate to a very small but finite value at large system size L in Fig. 5.

VII. FIDELITY WITH EXTENDED IMPURITY: CRITICAL EXPONENTIAL AOC

Next, we explore how the fidelity depends on the extension of the impurity at fixed total strength V_0, as defined by the impurity Hamiltonian (4). Clearly, in the limit when it extends over the whole system $M = L$, the eigenstates are not changed, and only the total energy is shifted by V_0/L, so that the fidelity is equal to one. Thus, one may expect that the fidelity increases as the the extension of the impurity M is increased at fixed total strength V_0. In fact, this is what happens for a periodic 1D tight-binding model for a weak impurity potential $V_0 = 0.1$, as seen in Fig. 18 in Appendix C, where the typical value of the fidelity and the upper bound $\exp(-I_A)$ are plotted as function of chain length L for different impurity extensions M. The typical fidelity increases with M, decaying more slowly with a power law of L, the larger M is. Similarly, in the metallic phase of the AA model for a weak impurity potential $V_0 = 0.1J$,, the typical and average fidelity become larger and decay more slowly with L as M is increased, as seen in Figs. 7(a) and 8(a), respectively, in accordance with the expectation formulated above. Averaging Eq. (5) over the phase ϕ we get the average Anderson integral for the extended impurity as

$$I_A = \frac{V_0^2}{2M^2} \sum_{n=1}^{N} \sum_{n'>N} \sum_{i,j\in S_M} \left\langle \frac{\psi_{ni}^* \psi_{n'i} \psi_{n'j}^* \psi_{nj}}{(E_{n'} - E_n)^2} \right\rangle_\phi . \tag{19}$$

As the phase difference of the wave-function amplitude between different sites varies with ϕ, averaging over the phase ϕ gives $\langle \psi_{ni} \psi_{nj}^* \rangle_\phi \approx \delta_{ij} |\psi_{ni}|^2$, so that we find in the metallic regime, where $|\psi_{ni}|^2 \sim L^{-1}$ that $I_A = 1/(2M)\rho_0^2 V_0^2 \ln N$, decaying with M, resulting in an increased fidelity with larger M, in qualitative agreement with the numerical results for the typical fidelity in the metallic regime [Fig. 7(a)].

In stark contrast to this, we find that in the critical phase of the AA model the fidelity is diminished more strongly with increasing extension M of the impurity, as seen in Fig. 7(b) where the typical fidelity is plotted, as well as in Fig. 8(b), where average fidelity is plotted, as function of length L for different extensions M for a fixed, weak impurity strength $V_0 = 0.1$ at the critical point $\lambda = 2.0$, averaged over 1000 sample realizations. Results at the critical point $\lambda = 2.0$ are replotted in a semilogarithmic plot in Fig. 9(a) for the typical fidelity and in Fig. 9(b) for the Anderson integral as function of length L for different impurity extension M for a fixed weak impurity strength $V_0 = 0.1$, averaged over 1000 sample realizations. Fits to power law and exponential dependence on L are plotted as indicated. For the largest extension $M = 7$ an exponential decay cannot be excluded. Thus, we may recover the analytically predicted exponential AOC in the critical phase [12], albeit only for an extended impurity. A possible explanation is that the magnitude of multipoint correlations, which we found to be responsible for masking the critical two-point correlations, may become diminished, for the extended impurity, so that the critical enhancement of two-point correlations dominates the typical fidelity for extended impurity, resulting in the exponential AOC in the critical phase. To get a better understanding of the result in the critical phase let us look at the distribution of the fidelity F in the critical phase $\lambda = 2.0$. For impurity strength $V_0 = 0.1$ averaged over 1000 realizations, for systems size $L = 1024$ the distribution is shown in Fig. 10(a). The distribution of the fidelity is found to be wide, as expected in the critical phase [12]. The probability that the ground state is not affected by the impurity, that the fidelity is close to one, is found to decrease with increasing M.

In the insulator phase $\lambda = 3$ for a fixed weak impurity strength $V_0 = 0.1$ the fidelity is decaying more strongly than in the other phases. With increasing extension M of the impurity the fidelity becomes larger, as seen in Figs. 7(c)

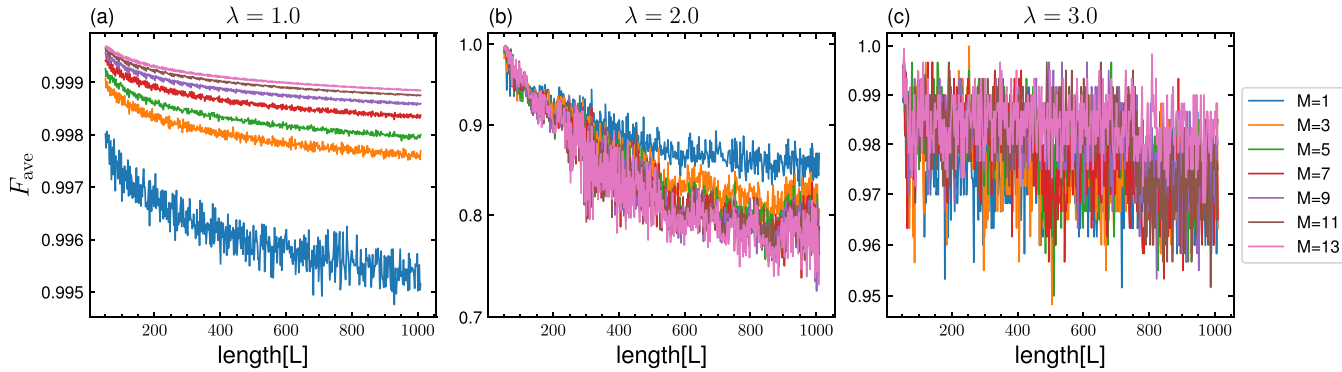

FIG. 8. Average value of fidelity $\langle F \rangle$ for the weak impurity with same parameters as in Fig. 7 with data sampled over 1000 realizations.

and 8(c), where the typical fidelity and average fidelity are plotted, respectively, as function of length L for different M averaged over 1000 sample realizations. The reason for that behavior might be that the effect on single-site localized states is smaller for an extended impurity, thereby diminishing the probability u that an occupied state becomes shifted to unoccupied states as the impurity is turned on, enhancing thereby the fidelity, according to the theory of the statistical exponential AOC as outlined in Sec. VI D.

For an extended impurity with strong amplitude $V_0 = 20J$, we find that the AOC is clearly exponential in the critical phase as seen in Fig. 11(b) for extension $M \gg 1$. We find that the larger the extension M, the more the fidelity becomes diminished and the stronger the exponential AOC becomes. This is confirmed by the distribution of the fidelity for such a strong impurity in the critical phase, as shown in Fig. 10(b).

In the metallic phase a strong impurity $V_0 = 20J$ is found to reduce the fidelity more strongly with increasing M, but the typical fidelity [Fig. 11(a)] and average fidelity [Fig. 12(a)] continue to decay with a power law in L for all M. A similar behavior is found for a strong impurity in the tight-binding model as shown in Appendix C, Fig. 19.

In the insulator phase Figs. 11(c) and 12(c) show a strong exponential AOC for the typical and average fidelity, respectively, which becomes stronger with the extension M of the impurity.

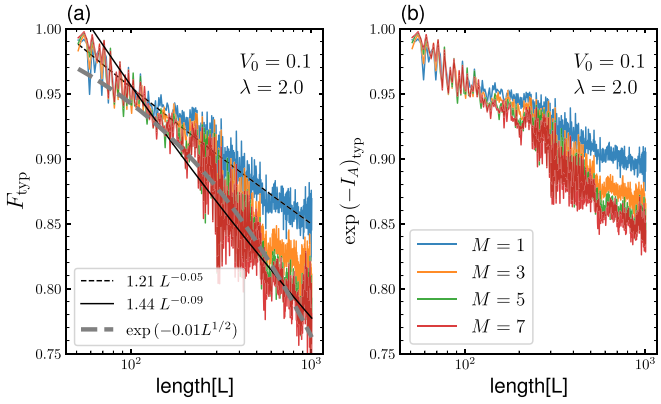

FIG. 9. (a) Typical fidelity and (b) exponential of negative Anderson integral as function of length L for different numbers of impurity sites M for weak impurity strength $V_0 = 0.1$ for the AA model at the critical point $\lambda = 2.0$ and averaged over 1000 sample realizations in a semilogarithmic plot. Fits to power law and exponential dependence on L are plotted as indicated. For the largest extension $M = 7$ an exponential decay cannot be excluded.

VIII. FIDELITY WITH PARAMETRIC PERTURBATION: PARAMETRIC EXPONENTIAL AOC

The concept of fidelity has been generalized to parametric perturbations of a quantum system. It has been successfully used to characterize quantum phase transitions [7]. Therefore, let us next study a perturbation which shifts the parameter λ for the AA model ($b = 0$) by a small amount $\delta\lambda$:

$$H_{\rm Pert} = \delta\lambda \sum_{i=1}^{L} \cos(2\pi Q i + \phi) c_i^+ c_i. \tag{20}$$

The effect of such a parametric perturbation has been recently studied in the AA model in Ref. [27] by calculating the so-called fidelity susceptibility $\chi_F(\lambda) = \lim_{\delta\lambda\to 0} -2 \log F/\delta\lambda^2$. We note that an upper bound for the fidelity susceptibility

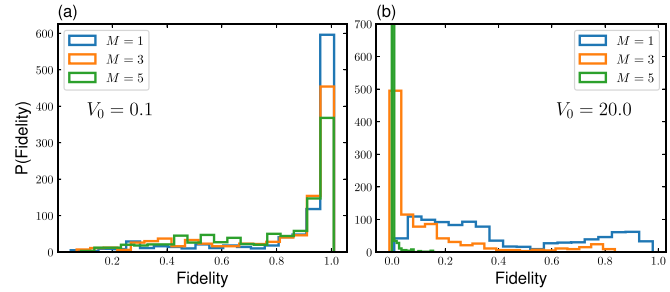

FIG. 10. The distribution of the fidelity F in the critical phase $\lambda = 2.0$ for impurity strength (a) $V_0 = 0.1$ and (b) $V_0 = 20$, averaged over 1000 realizations, for system size $L = 1024$ is shown for different extensions of the impurity M. The distribution is wide and more weight is shifted to small fidelity for increasing impurity strength and increasing M.

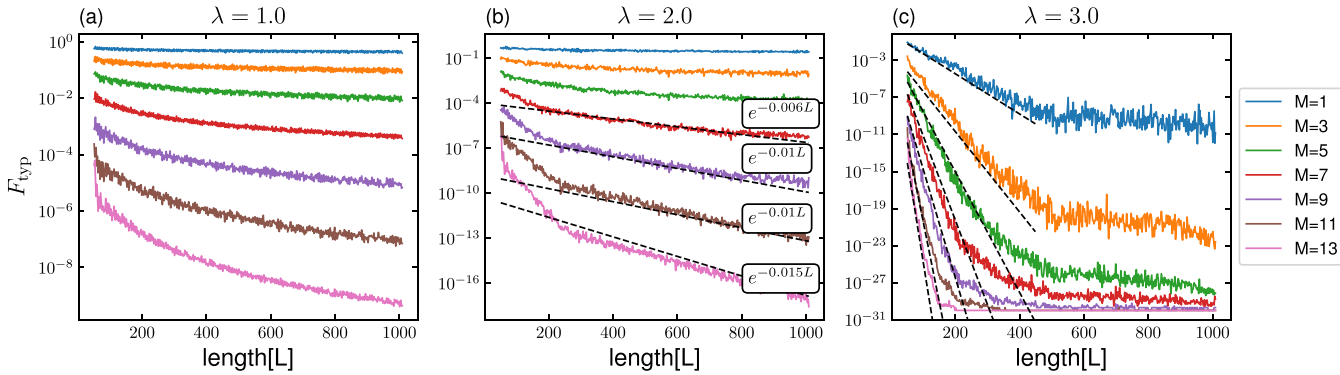

FIG. 11. Typical fidelity at filling $n = 0.309$ as function of lattice length for large impurity amplitude $V_0 = 20J$, for different extension M, each sampled over 1000 realizations. (a) In the metallic phase the fidelity decreases with increasing extension M and decays with a power law in L for all M. (b) In the critical phase the fidelity decays exponentially for $M > 1$. (c) In the insulator phase the fidelity decreases with increasing extension M and decays initially exponentially with L, saturating to a constant value at large L. The dashed lines are the fits to an exponential decay.

$\chi_F(\lambda)$ is given by the Anderson integral

$$\chi_F(\lambda) \leqslant \lim_{\delta\lambda\to 0} 2I_A/\delta\lambda^2$$

$$= \lim_{\delta\lambda\to 0} \frac{1}{\delta\lambda^2} \sum_{n=1}^{N} \sum_{n'>N} \frac{|\langle n|H_{\rm Pert}|n'\rangle|^2}{(E_{n'} - E_n)^2}$$

$$= \sum_{n=1}^{N} \sum_{l>N} \sum_{i,j} \frac{\cos(2\pi Qi + \phi)\cos(2\pi Qj + \phi)\psi^*_{ni}\psi_{nj}\psi_{li}\psi^*_{lj}}{(E_l - E_n)^2}, \tag{21}$$

where the indices n, l denote the unperturbed eigenstates.

In the critical phase, noting that local intensities are power-law correlated in energy, the dominating contributions come from the terms at the same locations $i = j$. Thus, we find

$$\chi_F(\lambda) \leqslant \sum_{n=1}^{N} \sum_{l>N} \sum_{i} \frac{\cos(2\pi Qi + \phi)^2 |\psi_{ni}|^2 |\psi_{li}|^2}{(E_l - E_n)^2}. \tag{22}$$

Averaging over the phase ϕ we thereby find approximating $\rho(E) \approx \rho_0$, and using $\Delta = \Delta_0 L^{-z}$

$$\chi_F(\lambda) \leqslant \frac{1}{2} \frac{\rho_0^2}{\gamma(1+\gamma)} \left(\frac{D}{\Delta_0} L^z\right)^{\gamma} \sim L^{z\gamma}, \tag{23}$$

where for the AA model in the critical phase $\lambda_c = 2$, $\gamma = \frac{1}{2}$.

Figure 13 shows the results for average (upper figure) and typical (lower figure) fidelity of a parametric perturbation with $\delta\lambda = 0.1$. As shown, in the metallic phase $\lambda < 2$ we find a slow decay in the average and typical fidelity which fits a slow exponential decay.

At the critical point $\lambda_c = 2$ the average and typical fidelity are clearly found to decay exponentially. The average fidelity is found to decay as $F_{\rm ave} \sim e^{-0.002L}$ and the typical as $F_{\rm typ} \sim e^{-0.003L}$. Thus, this gives for the typical fidelity susceptibility $\chi_F \approx 0.6L$, in good agreement with the analytical upper bound (23), which gives with $\gamma = \frac{1}{2}$, $\chi_F < 2L^{z/2}/3$, where z is the dynamical exponent, which we found numerically to be close to $z \approx 2$.

Using another approach near the quantum-critical point $\lambda_c = 2$, it was recently argued that the fidelity susceptibility scales with system size as $\chi_F(\lambda_c) \sim N^{2/\nu}$ [27], where ν is the correlation length critical exponent, given by $\nu \approx 0.89$ according to Ref. [28] and by $\nu \approx 0.95$ according to Ref. [29], which is also in some agreement with our numerical results.

In the localized phase $\lambda = 3$, both the average and typical fidelity show a very weak and strongly fluctuating dependence on L.

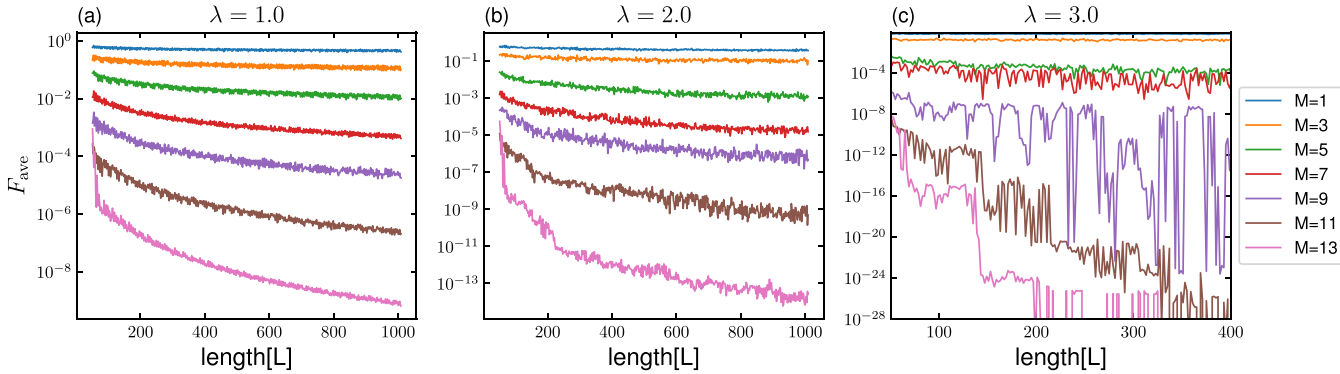

FIG. 12. Average fidelity $\langle F\rangle$ with same parameters as in Fig. 11. It is tentatively smaller than the typical value in Fig. 11 but shows the same trends with M and L, except that in the insulating phase the saturation value is orders of magnitude larger.

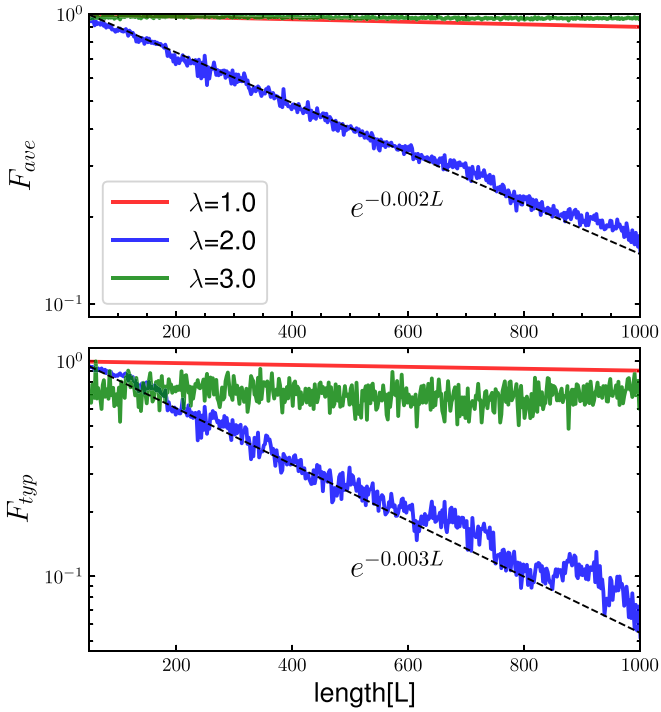

FIG. 13. Average (top) and typical (bottom) fidelities after a parametric perturbation in Eq. (3) with change $\delta\lambda = 0.1$, at fixed filling factor $n = 0.309$, and averaged over how 1000 samples. For the metallic phase $\lambda = 1$, both the average and the typical fidelities decay slowly, in the critical phase $\lambda = 2$ the decay is clearly exponential, as the fit shows (dashed line). In the insulator phase $\lambda = 3$ both typical and average the variation with L does not exceed its standard deviation.

IX. FIDELITY IN THE EXTENDED AA MODEL

The extended AA (EAA) model with Hamiltonian (3) for $b > 0$ has a mobility edge, as seen in Fig. 1 (right) where the inverse participation ratio IPR $= \sum_i |\psi_i|^4$ is plotted in a heat map as function of energy and quasiperiodicity parameter λ for the EAA model. The analytical formula for the mobility edge $E_{mb} = (2J\lambda)/b$ [2] (black solid line) is plotted in Fig. 1 (right), separating the extended phase with IPR $\to 0$ from the localized IPR $\to a/\xi$, where ξ is the localization length and a the lattice spacing. Since it was found analytically in Ref. [12] there is a critical exponential AOC at a mobility edge, let us explore whether it exists in the EAA model.

First, let us consider a single-site impurity $M = 1$ with weak potential $V_0 = 0.1$. In our calculation we set $b = 0.2$ and $\lambda = 2.0J$. We choose half-filling $n = N/L = 0.5$ so that the Fermi energy is at the mobility edge $E_{mb} = 0$ (see Fig. 1). In Fig. 14 we plot both the average and typical fidelity. The fit with a power law in system size L (black line) is good for the average fidelity. The typical fidelity shows a much smaller value for all system sizes with a stronger decay with L. The decay becomes stronger at larger L, deviating a power law, and possibly indicating an exponential AOC, as the fit to the stretched exponential $\exp(-cL^{1/2})$ as predicted by the analytical theory (the gray dashed line, where c is fitted as indicated in the legend) becomes better for large L.

Compared with the single-site impurity with weak potential $V_0 = 0.1J$ in the AA model, $b = 0$, in the critical phase $\lambda_c = 2$, shown in Fig. 3(a), the average fidelity is of similar magnitude in the EAA model at the mobility edge (Fig. 14), while the typical fidelity is smaller and decays faster in the EAA model at the mobility edge (Fig. 14), indicating an exponential AOC.

We depicted the average and typical value of $\exp(-I_A)$ in Fig. 14(b) and find that it gives, as expected, an upper bound for the fidelity for the whole range of system sizes explored. But, we note that the difference between the average and typical values is not as profound as for the fidelity itself.

We also plot the average and typical gap, the difference between HOMO and LUMO energies $\Delta(V_0)$ [Eq. (13)] for the extended AA model at the mobility edge in Fig. 14(c). For both average and typical, we find a power-law decay with L with dynamical exponent $z > 1$. Interestingly, the decay of the gap is stronger for the typical than the average gap, indicating a wide distribution of that gap. This is in contrast to the result for the gap (13) in the critical regime in the AA model, where the average and typical gaps showed a similar magnitude and decay (see Fig. 4).

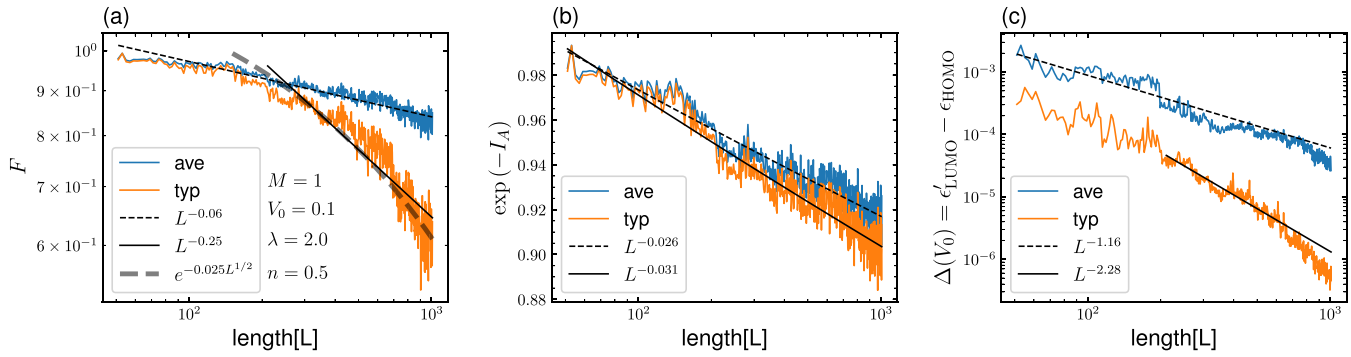

FIG. 14. For a single-site impurity $M = 1$ in the extended AA model at the mobility edge for $\lambda_c = 2.0$, $b = 0.2$, at half-filling $n = 0.5$, so that the energy is at the mobility edge $E_{mb} = 0$, (a) average and typical fidelity as function of length L with a single impurity of strength $V_0 = 0.1$. The black solid and dashed lines are fits to power laws, the gray dashed line a fit to an exponential function, as given in the legend. (b) Average and typical value of $\exp(-I_A)$, where I_A is the Anderson integral (5). (c) Average and typical value of the gap $\Delta(V_0)$ [Eq. (13)] as function of system size L. The dashed and solid lines are fits to power laws, as given in the legend. All results are averaged over 1000 sample realizations.

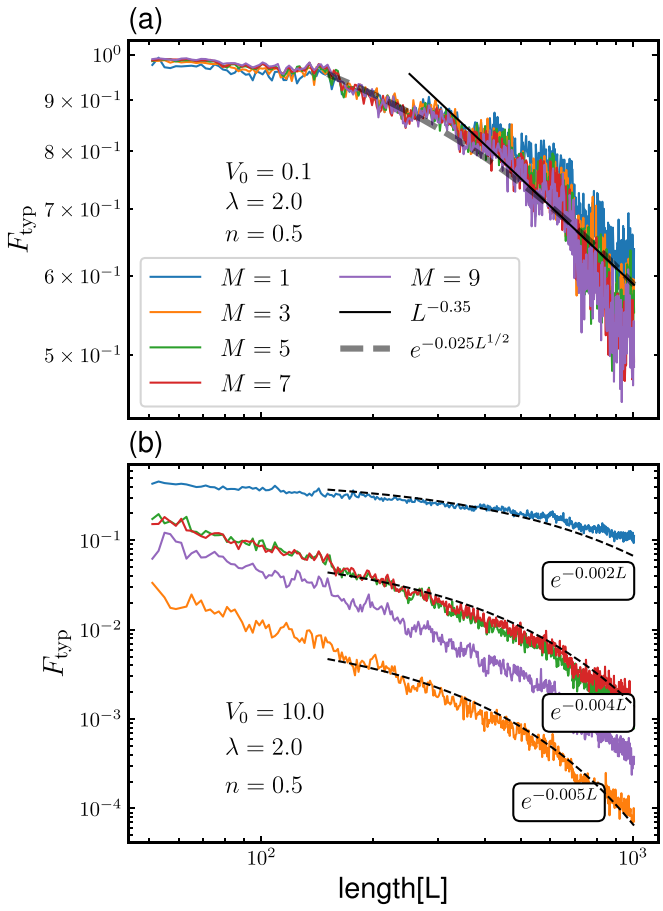

FIG. 15. Typical fidelity for an extended impurity for the extended AA model at the mobility edge for $\lambda_c = 2.0$, corresponding to half-filling $n = 0.5$, versus length L for different extension M. Impurity strength (a) $V_0 = 0.1$ and (b) $V_0 = 10$. All data averaged over 1000 sample realizations. Fitted curves are shown in solid or dashed black lines

Finally, let us consider the fidelity in the EAA model at its mobility edge with an impurity extended over M sites. In Figs. 15(a) and 15(b) we present the typical fidelity for a weak impurity strength $V_0 = 0.1$ and a strong one $V_0 = 10$, respectively. For the weak impurity [Fig. 15(a)] the typical fidelity is found to decay with system size L to smaller values, the larger the extension of the impurity M is, with deviations from a fit to a power law (black line, as given in the legend) at large L, where a fit to a stretched exponential (gray dashed line, as given in the legend), becomes better with larger extension M. For the strong impurity we observe in Fig. 15(b) a smaller typical fidelity is found, decaying exponentially with system size, as fitted by the dashed lines (as given in the legend), similarly as for a strong impurity in the critical AA model in Fig. 11(b).

X. CONCLUSION

While we do not find evidence for the predicted exponential AOC in the critical regime of the AA model for a weak single-site impurity, but rather find that the fidelity decays with a power law in the critical phase, we find indications for a stretched exponential decay of the fidelity at the mobility edge of the EAA model. The decay of the fidelity becomes stronger with stronger impurity strength, and the deviations from power-law behaviors more pronounced. For an extended impurity, we find clear evidence for an exponential AOC both at the quantum-critical point of the AA model and at the mobility edge of the extended AA model and suggest an explanation for this finding. By reexamination of the analytical derivation we identify nonperturbative corrections due to the impurity potential and multipoint correlations among wave functions as possible causes for the absence of the exponential AOC in the critical phase for a weak impurity in the AA model.

We find a different kind of exponential AOC in the insulator phase for which we give a statistical explanation, similar to that which was given in Ref. [14] for an adiabatic perturbation in an insulator phase, a mechanism which is profoundly different from the AOC in metals, where it is the coupling to a continuum of states which yields to the power-law suppression of the fidelity.

Furthermore we consider a parametric perturbation to the AA model, and find an exponential AOC numerically, in agreement with an analytical derivation which we provide here.

It has been suggested that the orthogonality catastrophe can be studied in ensembles of ultracold atoms in a controlled way [11]. Indeed, since the extended AA model was introduced and suggested to be experimentally realized in atomic optical lattices and photonic wave guides [2], it was recently realized in synthetic lattices of laser-coupled atomic momentum modes, and demonstrated to have a mobility edge [30]. We therefore hope that our analysis will provide guidance for the experimental study of the fidelity and the AOC in these systems. Furthermore, this opens new pathways for the study of nonequilibrium quantum dynamics. We note that our results can be extended to interacting disordered fermion systems, as multifractality exists even in strongly interacting disordered systems [31].

ACKNOWLEDGMENTS

We gratefully acknowledge the support from Deutsche Forschungsgemeinschaft (DFG) Grant No. KE-807/22-1, Project No. 408309204. We thank E. Demler for stimulating discussions, initiating this study, and K. Slevin for stimulating discussions and useful comments. We appreciate H. Arefi, as some parts of computation were run on his private cluster.

APPENDIX A: DERIVATION OF THE UPPER BOUND FOR QUANTUM FIDELITY

When the single-particle states of a Fermi system are $|n\rangle = c_n^+|0\rangle$, the ground state of N fermions is given by $|\psi\rangle = \prod_{n=1}^{N} c_n^+|0\rangle$. Adding an impurity, the single-particle states are changed to $|n'\rangle = c_{n'}^+|0\rangle$, so that the ground state becomes $|\psi'\rangle = \prod_{n'=1}^{N} c_{n'}^+|0\rangle$. The fidelity is given by the absolute value of the scalar product $F = |\langle\psi|\psi'\rangle| = |\langle 0|\prod_{n=1}^{N} c_n \prod_{n'=1}^{N} c_{n'}^+|0\rangle|$. Defining the scalar product of single-particle states of the pure system and the system with perturbation $A_{nn'} = \langle n|n'\rangle$ and applying the anticommutation

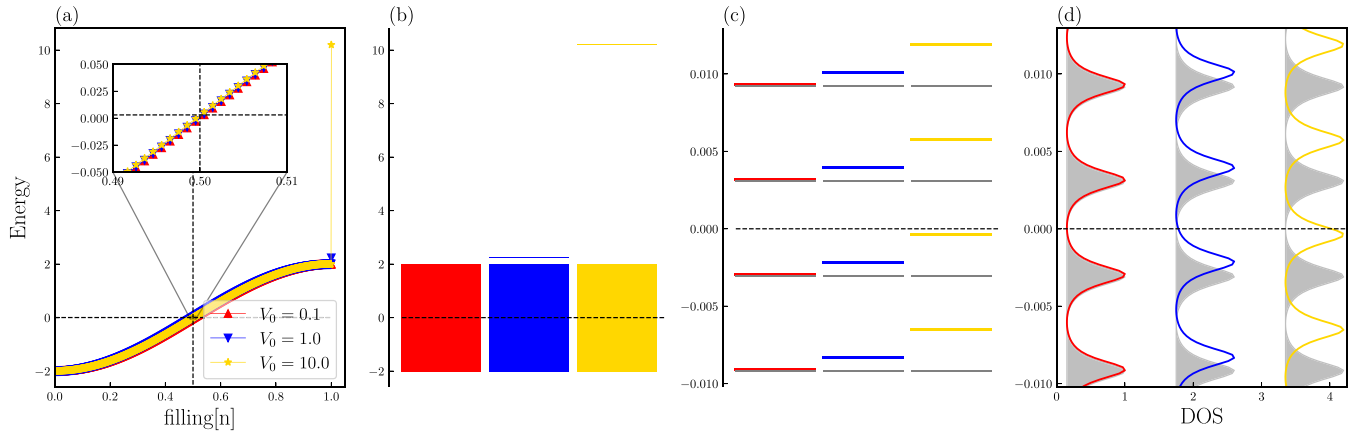

FIG. 16. (a) Energy level spectrum as function of filling factor n for a single impurity $M = 1$ with three different strengths V_0 (as displayed by the colored symbols). The dashed line indicates the filling of $n = 0.5$, corresponding without an impurity to Fermi energy $E_F/J = 0$. Inset: zoom close to the Fermi energy. (b), (c) Show a full and zoomed energy level diagram, with (colored) and without (gray) impurity. For $V_0 = 1.0$ and for $V_0 = 10.0$ the formation of a bound state outside of the band can be seen in (b). (d) Shows the density of states (DOS) as a function of energy close to Fermi energy with broadening $\eta = 1.0 \times e^{-5}$.

relations for c_n, c_n^+, we can write the fidelity as

$$F = |\det_{n,n' \leqslant N} A|. \tag{A1}$$

$A_{nn'}$ is for fixed n a normalized vector with $\sum_{n'} |A_{nn'}|^2 = 1$, However, since the summation in the fidelity F is restricted, and $|n'\rangle = \sum_{n \leqslant N} A_{nn'}|n\rangle + \sum_{n>N} A_{nn'}|n\rangle$, only those vector components with $n \leqslant N$ contribute to the fidelity F. This means that the determinant is taken of a square matrix with column vectors which are not normalized. However, we can normalize each column vector by multiplying it with $k_{n'} = (1 - \sum_{n>N} |A_{nn'}|)^{-1/2}$ and get the identity

$$F = \prod_{n' \leqslant N} \left(1 - \sum_{n>N} |A_{nn'}|^2\right)^{1/2} \det\left(A \prod_{n' \leqslant N} k_{n'}\right). \tag{A2}$$

Since the second factor is now a determinant with normalized column vectors, it cannot exceed one, but can be smaller, so that $\det(A \prod_{n' \leqslant N} k_{n'}) < 1$, and therefore

$$\begin{aligned} F &< \prod_{n' \leqslant N} \left(1 - \sum_{n>N} |A_{nn'}|^2\right)^{1/2} \\ &< \exp\left(-\frac{1}{2} \sum_{n' \leqslant N} \sum_{n>N} |A_{nn'}|^2\right). \end{aligned} \tag{A3}$$

APPENDIX B: THE ANDERSON SUM

When the unperturbed system has the Hamiltonian operator H_0 with eigenstates $|n\rangle$ determined by the Schrödinger equation $H_0|n\rangle = E_n|n\rangle$, adding an impurity with Hamiltonian H_{imp} [Eq. (4)] with potential strength V_0 changes the eigenstates to $|n'\rangle$ as determined by $(H_0 + H_{\text{imp}})|n'\rangle = E_{n'}|n'\rangle$. Multiplying the left with $\langle n|$ we thus get the identity

$$\langle n|n'\rangle = \frac{1}{E_{n'} - E_n} \langle n|H_{\text{imp}}|n'\rangle. \tag{B1}$$

Thus, for a local impurity $V = V_0 \delta(\mathbf{r} - \mathbf{x})$, we find

$$\begin{aligned} I_A &= \frac{1}{2} \sum_{n \leqslant N, n'>N} |\langle n|n'\rangle|^2 \\ &= \frac{1}{2} \sum_{n \leqslant N, n'>N} \frac{1}{(E_{n'} - E_n)^2} |\langle n|V|n'\rangle|^2 \\ &= \frac{V_0^2}{2} \sum_{n \leqslant N, n'>N} \frac{|\psi_n(\mathbf{x})|^2 |\psi_{n'}(\mathbf{x})|^2}{(E_{n'} - E_n)^2}, \end{aligned} \tag{B2}$$

where $|\psi_n(\mathbf{x})|^2 = |\langle n|\mathbf{x}\rangle|^2$, $|\psi_{n'}(\mathbf{x})|^2 = |\langle n'|\mathbf{x}\rangle|^2$ is the intensity with and without the additional impurity at postion $\mathbf{x}$.

APPENDIX C: BENCHMARK MODEL

In this Appendix, the tight-binding model is revisited numerically as a benchmark. We consider Hamiltonian $H = J \sum_i (c_i^\dagger c_i + \text{H.c.})$ and introduce the impurity as is defined in the main text in Eq. (4).

Figure 16(a) shows the energy level spectrum as function of filling factor n for a single impurity $M = 1$ with three different strengths V_0 (as displayed by the colored symbols). The dashed line indicates the filling of $n = 0.5$, corresponding without an impurity to the Fermi energy $E_F/J = 0$. Inset shows a zoom close to the Fermi energy. Figures 16(b) and 16(c) show a full and zoomed energy level diagram, with and without impurity. The case without impurity is drawn in a gray color. It can be seen that a bigger impurity strength results in stronger shifts of the energy close to the Fermi energy, which do not exceed the magnitude of the level spacing. For $V_0 = 1.0$, and for $V_0 = 10.0$ the formation of a bound state outside of the band can be seen in Fig. 16(b). Figure 16(d) shows the density of states (DOS) as a function of energy close to Fermi energy.

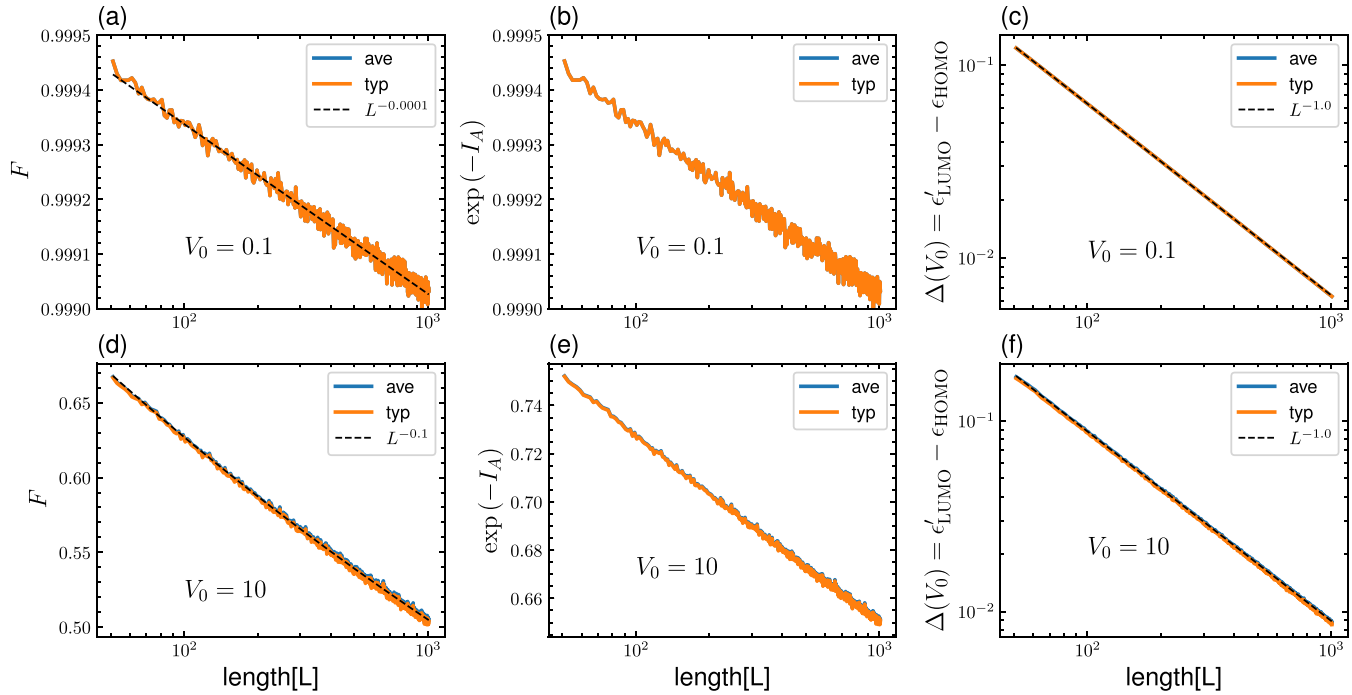

FIG. 17. (a), (d) Average and typical fidelity, (b),(e) Anderson integral and (c), (f) level spacing as a function of chain length, for the tight-binding model with a single impurity $M = 1$ positioned randomly on the chain for two impurity strengths $V_0 = 0.1,\ 10$. Data averaged over 1000 realizations. Black dashed lines are fitted curves as given in the figure legends. For impurity strength $V_0 = 0.1$, we find a power-law decay ($L^{-0.0001}$) for both fidelity and $\exp(-I_A)$. For the strong impurity case $V_0 = 10$, the fidelity decays much faster with system size ($L^{-0.1}$) and is smaller than $\exp(-I_A)$ for all system sizes considered. For both weak and strong impurities the gap Δ is independent of the impurity strength and decays as L^{-1}.

In Fig. 17 we show the numerical results for the typical and average fidelity F, the Anderson integral I_A, and the energy level spacing Δ as function of system size L for two impurity strengths $V_0 = 0.1,\ 10$. We considered a single impurity and averaged over its randomly chosen position. The typical and average fidelities are found to be indistinguishable, as expected for this clean model. For impurity strength $V_0 = 0.1$, we find a power-law decay fitted with $L^{-0.0001}$ for both fidelities and $\exp(-I_A)$ as function of system size L. We noticed that fidelity indeed never exceeds $\exp(-I_A)$, confirming that it provides an upper bound for the fidelity. For the strong impurity case $V_0 = 10$, the fidelity decays much faster with system size, fitted with $L^{-0.1}$. For both weak and strong impurities the level spacing Δ is independent of the impurity strength and decays as L^{-1}.

In Figs. 18 and 19 we show the results for an extended impurity for weak and strong potential, respectively. For the weak strength $V_0 = 0.1$, we observe that the fidelity decays

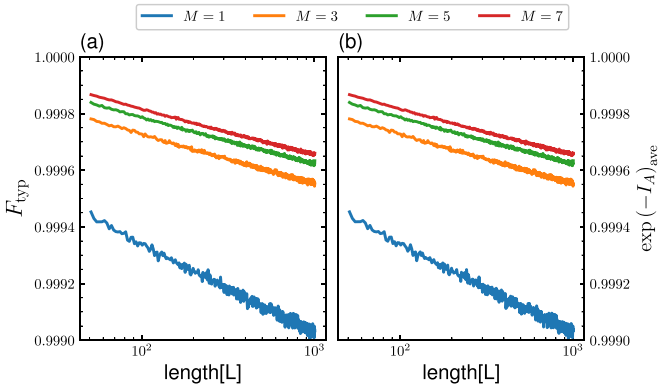

FIG. 18. Typical value of (a) the fidelity and (b) the upper bound $\exp(-I_A)$ for a 1D tight-binding model plotted with added impurity (4) as function of chain length L for different impurity extensions M for fixed impurity strength $V_0 = 0.1$. Data averaged over 1000 realizations.

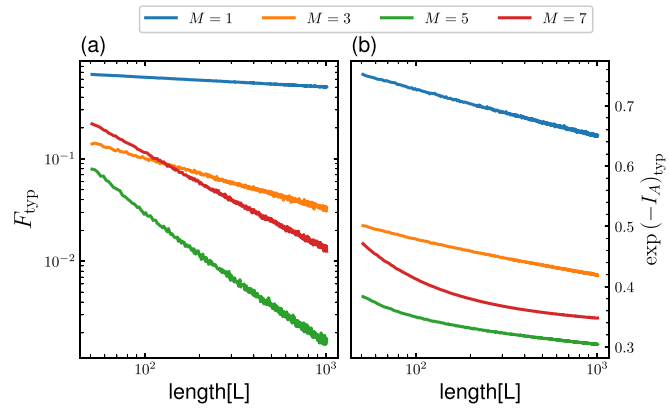

FIG. 19. Same as Fig. 18, but for impurity strength $V_0 = 10$.

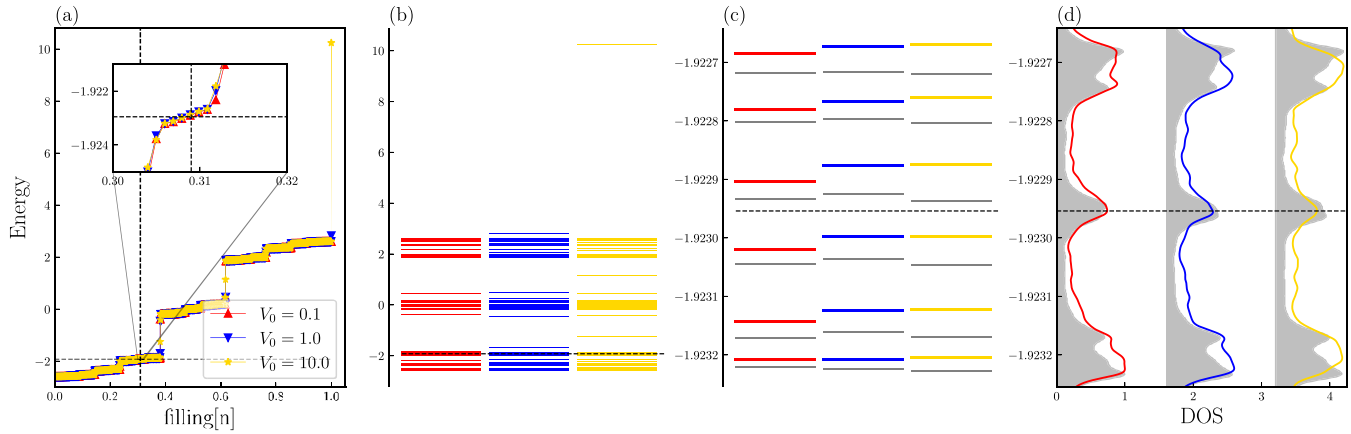

FIG. 20. Same as Fig. 2 but with averaging over 200 realizations.

with a power law with system size. It decays more slowly the more extended the impurity is. This is in agreement with the fidelity behavior in the metallic phase of the (extended) AA model reported in the main text. For the strong impurity, however, as shown in Fig. 19, the typical fidelity is smaller for large extension $M > 1$, and deviations from power-law decay are observable.

APPENDIX D: AVERAGE ENERGY SPECTRUM

In this Appendix, we present the average numerical results of energy spectrum of the AA model reported in the main text. Figure 20 shows the energy diagram and density of states as function of energy E, as averaged over the random phases ϕ in the Hamiltonian (3) for $b = 0$ and $\lambda = 2$ of 200 realizations.

[1] P. W. Anderson, Phys. Rev. Lett. **18**, 1049 (1967).
[2] S. Ganeshan, J. H. Pixley, and S. Das Sarma, Phys. Rev. Lett. **114**, 146601 (2015).
[3] P. Nozieres and C. T. de Dominicis, Phys. Rev. **178**, 1097 (1969).
[4] B. Altshuler and A. Aronov, Zh. Eksp. Teor. Fiz. **77**, 2028 (1979) [Sov. Phys. JETP **50**, 968 (1980)].
[5] J. M. Kinaret, Y. Meir, N. S. Wingreen, P. A. Lee, and X. G. Wen, Phys. Rev. B **46**, 4681 (1992).
[6] A. V. Shytov, L. S. Levitov, and B. I. Halperin, Phys. Rev. Lett. **80**, 141 (1998).
[7] L. C. Venuti, H. Saleur, and P. Zanardi, Phys. Rev. B **79**, 092405 (2009).
[8] S. Yang, K. Sun, and S. Das Sarma, Phys. Rev. B **85**, 205124 (2012).
[9] O. Lychkovskiy, O. Gamayun, and V. Cheianov, Phys. Rev. Lett. **119**, 200401 (2017).
[10] S. R. Das, *Quantum Quench and Universal Scaling*, Oxford Research Encyclopedia of Physics (Oxford University Press, 2020), p. 12.
[11] M. Knap, A. Shashi, Y. Nishida, A. Imambekov, D. A. Abanin, and E. Demler, Phys. Rev. X **2**, 041020 (2012).
[12] S. Kettemann, Phys. Rev. Lett. **117**, 146602 (2016).
[13] Y. Gefen, R. Berkovits, I. V. Lerner, and B. L. Altshuler, Phys. Rev. B **65**, 081106(R) (2002).
[14] V. Khemani, R. Nandkishore, and S. L. Sondhi, Nat. Phys. **11**, 560 (2015).
[15] D.-L. Deng, J. H. Pixley, X. Li, and S. Das Sarma, Phys. Rev. B **92**, 220201(R) (2015).
[16] S. Aubry and G. André, Ann. Israel Phys. Soc. **3**, 133 (1980).
[17] H. Hiramoto and M. Kohmoto, Int. J. Mod. Phys. B **06**, 281 (1992).
[18] A.-K. Wu, S. Gopalakrishnan, and J. H. Pixley, Phys. Rev. B **100**, 165116 (2019).
[19] F. Wegner, Z. Phys. B **36**, 209 (1980); H. Aoki, J. Phys. C: Solid State Phys. **16**, L205 (1983); C. Castellani and L. Peliti, J. Phys. A: Math. Gen. **19**, L1099 (1986); M. Schreiber and H. Grußbach, Phys. Rev. Lett. **67**, 607 (1991); M. Janssen, Int. J. Mod. Phys. B **08**, 943 (1994).
[20] J. T. Chalker, Phys. A (Amsterdam) **167**, 253 (1990); V. E. Kravtsov and K. A. Muttalib, Phys. Rev. Lett. **79**, 1913 (1997); J. T. Chalker, V. E. Kravtsov, and I. V. Lerner, JETP Lett. **64**, 386 (1996); T. Brandes, B. Huckestein, and L. Schweitzer, Ann. Phys. (Leipzig) **508**, 633 (1996); V. E. Kravtsov, *ibid.* **511**, 621 (1999); V. E. Kravtsov, A. Ossipov, O. M. Yevtushenko, and E. Cuevas, Phys. Rev. B **82**, 161102(R) (2010); V. E. Kravtsov, A. Ossipov, and O. M. Yevtushenko, J. Phys. A: Math. Theor. **44**, 305003 (2011).
[21] E. Cuevas and V. E. Kravtsov, Phys. Rev. B **76**, 235119 (2007).
[22] M. V. Feigel'man, L. B. Ioffe, V. E. Kravtsov, and E. A. Yuzbashyan, Phys. Rev. Lett. **98**, 027001 (2007); M. V. Feigel'man, L. B. Ioffe, V. E. Kravtsov, and E. Cuevas, Ann. Phys. **325**, 1390 (2010).
[23] A. Duthie, S. Roy, and D. E. Logan, Phys. Rev. B **104**, 064201 (2021).
[24] E. N. Economou, *Green's Functions in Quantum Physics* (Springer, Berlin, 1983).

[25] N. Moure and S. Haas (unpublished).
[26] K. Slevin (unpublished).
[27] B.-B. Wei, Phys. Rev. A **99**, 042117 (2019).
[28] M. Thakurathi, D. Sen, and A. Dutta, Phys. Rev. B **86**, 245424 (2012).
[29] T. Cookmeyer, J. Motruk, and J. E. Moore, Phys. Rev. B **101**, 174203 (2020).
[30] F. A. An, K. Padavic, E. J. Meier, S. Hegde, S. Ganeshan, J. H. Pixley, S. Vishveshwara, and B. Gadway, Phys. Rev. Lett. **126**, 040603 (2021).
[31] M. Amini, V. E. Kravtsov, and M. Müller, New J. Phys. **16**, 015022 (2014); I. S. Burmistrov, I. V. Gornyi, and A. D. Mirlin, Phys. Rev. Lett. **111**, 066601 (2013); Y. Harashima and K. Slevin, Phys. Rev. B **89**, 205108 (2014).